Highly Stable Monolayer Resists for Atomic Layer Deposition on Germanium and Silicon

Rong Chen[†] and Stacey F. Bent*[,‡]

Department of Chemistry and Department of Chemical Engineering, Stanford University, Stanford, California 94305

Received April 3, 2006. Revised Manuscript Received May 12, 2006

In this paper, 1-alkenes and 1-alkynes are investigated for a new class of monolayer resists formed on the hydrogen-terminated surfaces of both germanium and silicon. A series of 1-alkenes and 1-alkynes with different chain lengths are explored as deactivating agents for atomic layer deposition of HfO_2 and Pt films. It is shown that to achieve satisfactory blocking of atomic layer deposition, densely packed, highly hydrophobic monolayers must be formed. A mechanism for the film formation and blocking processes is discussed and compared with that of alkylsilane-based self-assembled monolayer resists.

Introduction

Ge is a material important to the history of the semiconductor industry. The first semiconductor transistor and the first integrated circuit were both fabricated based on Ge.[1] However, the lack of a stable native oxide for Ge, unlike Si, hinders the formation of a good interface at the semiconductor, which in turn leads to a higher density of interfacial traps and surface states.[2] Silicon ultimately became the predominant semiconductor material because of its stable oxide and excellent $Si-SiO_2$ interfacial properties. With continuing device scaling and recent trends in gate dielectrics evolution, there has currently been renewed interest in utilizing germanium to complement silicon in devices due to its higher carrier mobility.[3] Many studies have been carried out using Ge as a channel material in high-speed field-effect transistors (FETs).[4−8]

The main trend in the evolution of the gate dielectric has been a shift to higher dielectric constant materials. Specifically, the drive to reduce the leakage current caused by direct electron tunneling from the gate to the channel in metal oxide semiconductor FETs (MOSFETs) has led to efforts to replace SiO_2 by high-κ dielectric layers. When SiO_2 is replaced by a high-κ material in the MOSFET structure, Ge once again becomes a viable semiconductor material, and the Ge-based MOSFETs produced using high-κ dielectrics have demonstrated very good electrical properties.[9] With the introduction of high-κ materials as gate dielectrics to replace conventional SiO_2, part of the leakage current problem can be mitigated. Nevertheless, the latest research shows that new gate electrode materials will also need to be developed. As a result of the current thermal budget requirements for dopant activation, conventional doped polysilicon gate electrodes deplete a few angstroms at the interface with SiON and SiO_2 gate dielectrics, and the situation is even worse for high-κ materials.[10] To decrease electrode depletion, metals are being evaluated as gate electrode materials for good compatibility with high-κ dielectrics for future MOS devices.

In this study, we examine the possibility of using a novel area-selective atomic layer deposition (ALD) process to deposit a model metal high-κ gate stack. Among various methods for depositing ultrathin and uniform films of high-κ gate dielectrics and gate metals, ALD has received considerable attention. It is a powerful film growth technique that employs a sequence of self-limiting surface reaction steps to afford sub-nanometer control of the growth process.[11,12] Typically, the process permits nanoscale control in the vertical direction. On the other hand, the area-selective ALD technique enables micro- and, ultimately, nanoscale definition of the lateral structure for three-dimensional nano-patterning. Area-selective ALD is an additive process in which material is deposited only where needed.[13] We strive to use this

* To whom correspondence should be addressed. Phone: 650-723-0385. Fax: 650-723-9780. E-mail: sbent@stanford.edu.
[†] Department of Chemistry.
[‡] Department of Chemical Engineering.

(1) Pierret, R. F. *Semiconductor Device Fundamentals*; Addison-Wesley Publishing Co., Inc.: Reading, MA, 1996.
(2) Balk, P. *The Si-SiO$_2$ System*; Elsevier: Amsterdam, 1988; Vol. 32, p 2.
(3) Kittle, C. *Introduction to Solid State Physics*, 7th ed.; John Wiley & Sons: New York, 1996.
(4) Chui, C. O.; Ito, F.; Saraswat, K. C. *IEEE Electron Device Lett.* **2004**, *25*, 613.
(5) Chui, C. O.; Ramanathan, S.; Triplett, B. B.; McIntyre, P. C.; Saraswat, K. C. *IEEE Electron Device Lett.* **2002**, *23*, 473.
(6) Maiti, C. K.; Mandal, S. K.; Chakraborty, S. *Microelectron. Eng.* **2005**, *81*, 206.
(7) Kalavade, P.; Shulze, J. *Ge in main-stream CMOS: a future or fancy?*; Device Research Conference, Notre Dame, IN, June, 21−23, 2004, IEEE: Piscataway, NJ, 2004; Vol. 1, p 189.
(8) Singer, P. *Semicond. Int.* **2005**, *28*, 46.
(9) Bai, W. P.; Lu, N.; Liu, J.; Ramirez, A.; Kwong, D. L.; Wristers, D.; Ritenour, A.; Lee, L.; Antoniadis, D. *Dig. Tech. Pap. Symp. VLSI Technol.* **2003**, 121.
(10) Gusev, E. P.; Buchanan, D. A.; Cartier, E.; Kumar, A.; DiMaria, D.; Guha, S.; Callegari, A.; Zafar, S.; Jamison, P. C.; Neumayer, D. A.; Copel, M.; Gribelyuk, M. A.; Okorn-Schmidt, H.; D'Emic, C.; Kozlowski, P. *Tech. Dig. Int. Electron Device Meet.* **2001**, 451.
(11) Ritala, M.; Kukli, K.; Rahtu, A.; Ralsanen, P. I.; Leskla, M.; Sajavaara, T.; Keinonen, J. *Science* **2000**, *288*, 319.
(12) Ritala, M.; Leskela, M. *Handbook of Thin Film Materials*; Academic Press: San Diego, 2002; Vol. 1, p 103.
(13) Chen, R.; Porter, W. D.; Kim, H.; McIntyre, P. C.; Bent, S. F. *Appl. Phys. Lett.* **2005**, *86*, 191910.

10.1021/cm0607785 CCC: $33.50 © 2006 American Chemical Society
Published on Web 07/12/2006

process to ultimately deposit HfO_2 and Pt selectively at the gate region with only one pre-patterning step.

We have chosen hafnium dioxide (HfO_2) and platinum (Pt) as the model high-κ dielectric and metal electrode material, respectively. HfO_2 has drawn significant attention as a promising high-κ material because of its high-κ value and wide band gap (~5.68 eV).[14] Pt is a promising electrode material for dynamic random access memories (DRAMs) for its high chemical stability in oxidizing atmosphere and excellent electrical properties.[15,16] It also has a high work function (5.6 eV) and is compatible with high-κ dielectrics.[17]

To develop the area-selective ALD process, it is important to find a robust resist that can block deposition. Recently, self-assembled monolayers (SAMs) have been shown to act as effective resists for the ALD process on Si substrates.[18−23] SAMs are monolayer organic films that form spontaneously on solid surfaces, and they are well-known to modify the physical, chemical, and electrical properties of semiconducting, insulating, and metallic surfaces.[24] There are two main categories of SAMs that can form covalent bonds on semiconductor surfaces. One class is the organosilane based SAMs which form Si−O linkages with substrate hydroxyl groups. This type of SAM relies on the presence of a stable oxide layer on the substrate, for example, SiO_2. The other type of SAM attaches directly to the semiconductor surface atoms and does not require surface hydroxyl groups or an oxide. For example, 1-alkenes react with hydrogen-terminated Si or Ge substrates through a hydrosilylation or hydrogermylation reaction to form monolayers via direct Si−C or Ge−C covalent bonds.[25−27]

In previous studies of area-selective ALD using monolayer passivation, alkylsilane based SAMs were used as the resist for the ALD process on Si substrates.[18−23] This approach relied upon the presence of a stable oxide (SiO_2) layer for the SAM formation. However, if we wish to carry out the process on Ge, we can no longer depend on resists which require oxides for attachment, and hence other types of monolayer resists need to be investigated. In this paper, we explore the formation of a monolayer directly on hydrogen-terminated Ge using 1-alkene/1-alkyne hydrogermylation chemistry, which previous studies have shown exhibits good chemical and thermal stability,[28] and will characterize the efficiency of these monolayers in blocking both HfO_2 and Pt ALD. We also explore the analogous hydrosilylation process on hydrogen-terminated Si substrates, which we have recently shown to form monolayers that resist ALD.[29] The process sequence is illustrated in Scheme 1. In this process, monolayer resists are formed on Ge or Si via hydrogermylation or hydrosilylation, respectively, and the resists then prevent ALD on the semiconductor substrates. We will discuss the properties of the monolayer resists formed by different hydrogermylation/hydrosilylation methods (thermal and photochemical reactions) and correlate their properties with their performance as resists for HfO_2 and Pt ALD processes. This study will enable future direct patterning of these monolayer resists, high resolution lithography, and ultimately the area-selective ALD of the in situ gate stack of nanoscale devices.

Scheme 1. Schematic Illustration of Formation of Monolayer Resists by 1-Alkenes or 1-Alkyne on a Hydrogen-Terminated Semiconductor Substrate and Subsequent Blocking of the ALD Process

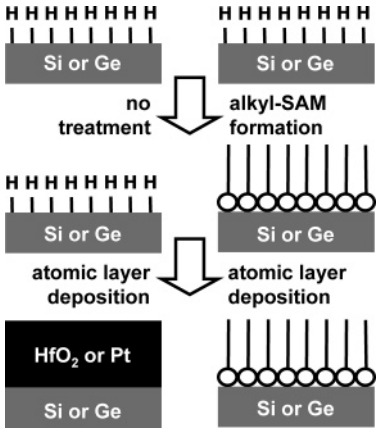

Experiments

1. SAM Preparation. *(a) Reagents.* All chemical reagents were purchased from Aldrich (Milwaukee, WI). Petroleum ether (PE, ACS reagent), ethanol (EtOH, ACS reagent), and dichloromethane (CH_2Cl_2, ACS reagent) were used as purchased. Mesitylene (98%), the 1-alkenes [1-octadecene (technical grade 90%), 1-hexadecene (technical grade 92%), 1-tetradecene (technical grade, 92%), 1-dodecene (95%), 1-decene (94%), and 1-octene (98%)], and the 1-alkynes [1-dodecyne (98%), 1-decyne (98%), and 1-octyne (97%)] were all distilled over CaH_2 by reduced pressure and stored with molecular sieves in Argon purged bottles.

(b) Wafers. Germanium sample substrates were cleaved from Ge(100) (n-type) and Ge(111) (n-type) wafers purchased from Umicore (Belgium). Silicon sample substrates were cut from Si(100) (p-type) (Si−Tech, Inc. Topsfield, MA) and Si(111) (n-type) (Mitsubishi Silicon American).

(c) Substrate Cleaning and Etching. Ge and Si samples were sonicated for at least 10 min in acetone and chloroform prior to etching. This cleaning serves to remove any particles generated during wafer cleaving. Subsequently, the samples were etched in HF solutions. For germanium etching, the Ge(100) and Ge(111) samples were oxidized in 30% hydrogen peroxide solution for 5

(14) Kang, L.; Jeon, Y.; Onishi, K.; Lee, B.; Qi, W.; Nieh, R.; Gopalan, S.; Lee, J. C. *Dig. Technol. Pap. Symp. VLSI Technol.* **2000**, 44.
(15) Hiratani, M.; Nabatame, T.; Matsui, Y.; Imagawa, K.; Kimura, S. *J. Electrochem. Soc.* **2001**, *148*, C524-7.
(16) Nayak, M.; Ezhilvalavan, S.; Tseng, T. Y. *Handbook of Thin Film Materials*; Academic Press: San Diego, 2001; Vol. 3, p 121.
(17) Wilk, G. D.; Wallace, R. M.; Anthony, J. M. *J. Appl. Phys.* **2001**, *89*, 5243.
(18) Chen, R.; Kim, H.; McIntyre, P. C.; Bent, S. F. *Appl. Phys. Lett.* **2004**, *84*, 4017.
(19) Chen, R.; Kim, H.; McIntyre, P. C.; Bent, S. F. *Mater. Res. Soc. Symp. Proc.* **2004**, *811*, 57.
(20) Chen, R.; Kim, H.; McIntyre, P. C.; Bent, S. F. *Chem. Mater.* **2005**, *17*, 536.
(21) Lee, J. P.; Sung, M. M. *J. Am. Chem. Soc.* **2004**, *126*, 28.
(22) Park, M. H.; Jang, Y. J.; Sung-Suh, H. M.; Sung, M. M. *Langmuir* **2004**, *20*, 2257.
(23) Yan, M.; Koide, Y.; Babcock, J. R.; Markworth, P. R.; Belot, J. A.; Marks, T. J.; Chang, R. P. H. *Appl. Phys. Lett.* **2001**, *79*, 1709.
(24) Ulman, A. *Chem. Rev.* **1996**, *96*, 1535.
(25) Buriak, J. M. *Chem. Rev.* **2002**, *102*, 1271.
(26) Linford, M. R.; Chidsey, C. E. D. *J. Am. Chem. Soc.* **1993**, *115*, 12631.
(27) Linford, M. R.; Fenter, P.; Eisenberger, P. M.; Chidsey, C. E. D. *J. Am. Chem. Soc.* **1995**, *117*, 3145.
(28) Choi, K.; Buriak, J. M. *Langmuir* **2000**, *16*, 7737.
(29) Chen, R.; Bent, S. F. *Adv. Mater.* **2006**, *18*, 1086.

min, followed by deionized (DI) water rinsing, and then etched in 10% aqueous HF for 2 min. This cycle was repeated three times to remove trace GeO_x species on the surface, as confirmed by XPS. For silicon, the samples were subjected to piranha cleaning (a fresh mixture of 30% H_2O_2 and 98% H_2SO_4 in a 3:7 volume ratio; caution, fresh piranha is hot and corrosive, use extreme caution when handling piranha solution) for 15 min before etching. The Si(100) samples were etched in 2% dilute HF solution for 2 min, and the Si(111) samples were etched in 40% NH_4F solution for 5 min. Both the 2% HF solution and 40% NH_4F solution were held under argon bubbling for at least 30 min before the etch to remove trace amounts of oxygen dissolved in the etchants.

(d) Monolayer Preparation. For Ge(100)-H and Ge(111)-H samples, neat 1-alkenes and 1-alkynes were used for both thermal and UV reactions. For Si(100)-H and Si(111)-H samples, 1-alkenes/1-alkynes in mesitylene (in a 1:2 volume ratio) solutions were used for the thermal and UV reactions.

(i) Thermal Method. In the thermal method, the reagent solution was placed in a small three-necked flask fitted with an argon inlet, a reflux condenser with a $CaCl_2$ tube, and a stopper. The solution was degassed by bubbling Ar through it for at least 1 h. Subsequently, a cleaned and freshly etched sample was placed into the flask and degassed with Ar for another 30 min. Then the Ar inlet was moved to a position just above the solution to change from an Ar-sparged system to a moderate purge gas flow. The entire reflux system was then heated at 220 °C for 2 h. Upon completion of the thermal reaction, the sample was removed from the solution and rinsed extensively with PE, EtOH, and CH_2Cl_2, sequentially.

(ii) Photochemical Method. The reagent was placed in a small quartz cuvette fitted with an Ar gas inlet and a needle outlet. The same degassing method was followed as for the thermal method. Following the degassing step, a UV lamp (ozone free double bore lamp, model no. 82-3309-2, Jelight Co., Inc., Irvine, CA) that was fixed at a distance of 0.5 cm from the reaction cuvette was turned on, and it irradiated the solution for 2 h. Upon completion of the photoreaction, the sample was removed from the solution and rinsed extensively with PE, EtOH, and CH_2Cl_2, sequentially.

2. ALD Process. The ALD precursors for HfO_2 deposition are high-purity tetrakis(dimethylamido)hafnium ($Hf(NMe_2)_4$) and DI water. The HfO_2 ALD process includes two self-limiting chemical reactions, repeated in the alternating ABAB sequences shown below:

$$Hf{-}OH^* + Hf(NMe_2)_4 \rightarrow Hf{-}O{-}Hf(NMe_2)_3{}^* + NHMe_2\uparrow \quad (A)$$

$$Hf{-}NMe_2{}^* + H_2O \rightarrow Hf{-}OH^* + NHMe_2\uparrow \quad (B)$$

where the asterisks represent the surface species.[30] The exposure times for $Hf(NMe_2)_4$ and water vapor were 0.1 and 0.2 s, respectively, followed by 3 min of nitrogen purge after each precursor was introduced into the reactor. For HfO_2 film growth, a total of 50 ALD cycles were applied on all samples. A 0.8 Å/cycle growth rate was observed on a chemical oxide-coated silicon substrate.

For Pt ALD, the precursors are high-purity (methylcyclopentadienyl)trimethylplatinum ($MeCpPtMe_3$) (Cp = cyclopentadienyl) and oxygen (here we use dry air as the oxygen source). The Pt ALD process includes two proposed self-limiting chemical reactions, repeated in the alternating ABAB sequences shown below:

$$Pt(s) + O_2(g) \rightarrow Pt\cdots O_x(ad) \quad (A)$$

$$CH_3C_5H_4Pt(CH_3)_3 + Pt\cdots O_x(ad) \rightarrow Pt(s) + CO_2(g)\uparrow + H_2O(g)\uparrow + \text{other byproducts}\uparrow \quad (B)$$

where the notation (ad) represents the surface species.[31,32] The exposure times for the platinum precursor and air were 3 and 2 s, respectively, followed by 60 and 45 s nitrogen purges after each precursor was introduced into the reactor. For Pt film growth, a total of 75 ALD cycles were applied on all samples. A 0.4 Å/cycle growth rate was observed on a chemical oxide-coated silicon substrate.

The ALD processes were carried out in a custom built cold-wall reactor with different chamber designs for the HfO_2 versus the Pt process. The pulse and purge times above were optimized for each individual process, as they are a function of parameters such as precursor vapor pressure, precursor reactivity, and reactor design. Ultrahigh purity compressed nitrogen gas was flowed at a rate of 200 sccm through the lines that connected precursor bubblers into the ALD reactor. The temperature of the ALD reactor was maintained at 250 °C for the HfO_2 process and 300 °C for the Pt process. The base pressure was maintained at 600 mTorr during the whole process.

3. Film Characterization. One of the most surface-sensitive and rapid techniques for judging the quality of a SAM is to measure the wetting properties of a SAM-coated substrate. Ellipsometry and X-ray photoelectron spectroscopy (XPS) provide information on film thickness and elemental composition, respectively. All three of these techniques provide a macroscopic view of the film properties averaged over a relatively large sampling area. Atomic force microscopy (AFM), on the other hand, provides nanoscale information on the film, which is useful in understanding the blocking mechanism of the monolayers toward the ALD precursors.

An FTA 2000 dynamic contact angle analyzer was used to measure the water contact angle (WCA). The WCAs reported in this paper are static angles. A sessile drop of Millipore Milli-Q water (resistivity = 18.2 MΩ·cm) with constant volume (20 μL) was applied onto the surface of each sample. At least four different points of each sample were measured to get the average value for the WCAs.

A Gaertner Scientific Corp. L116C He−Ne laser ellipsometer was used to measure the film thickness for this study. The incident angle for the ellipsometer is 70°. A refractive index of $n = 1.46$ was used for the organic films.[24] More than five points were measured on each sample to check the uniformity and to obtain an average value for the film thickness.

The XPS and AFM analyses were carried out in the facilities of the Geballe Laboratory for Advanced Materials (GLAM) at Stanford University. The XPS system used is an SSI S-Probe monochromatized spectrometer, with Al Kα radiation (1486 eV) as the source. This instrument permits high sensitivity and good energy resolution. All the spectra shown in this paper had a detection sensitivity of ~0.1 atomic percentage (atom %).

Surface morphology was investigated by AFM (Digital Instruments, Inc., Santa Barbara, CA). The surface morphology of the samples before and after ALD processing was compared to help elucidate the blocking mechanism and the film nucleation process. Contact mode AFM was used for Pt films, while tapping mode was used for SAMs and HfO_2 surfaces because tapping mode was found to damage the SAMs and HfO_2 films.

Results and Discussion

1. Octadecyl-Covered Substrates. Octadecyl-covered Ge(100) and Si(100) surfaces were prepared from the

(30) Hausmann, D. M.; Kim, E.; Becker, J.; Gordon, R. G. *Chem. Mater.* **2002**, *14*, 4350.
(31) Aaltonen, T.; Ritala, M.; Sajavaara, T.; Keinonen, J.; Leskela, M. *Chem. Mater.* **2003**, *15*, 1924.
(32) Aaltonen, T.; Ritala, M.; Tung, Y. L.; Chi, Y.; Arstila, K.; Meinander, K.; Leskela, M. *J. Mater. Res.* **2004**, *19*, 3353.

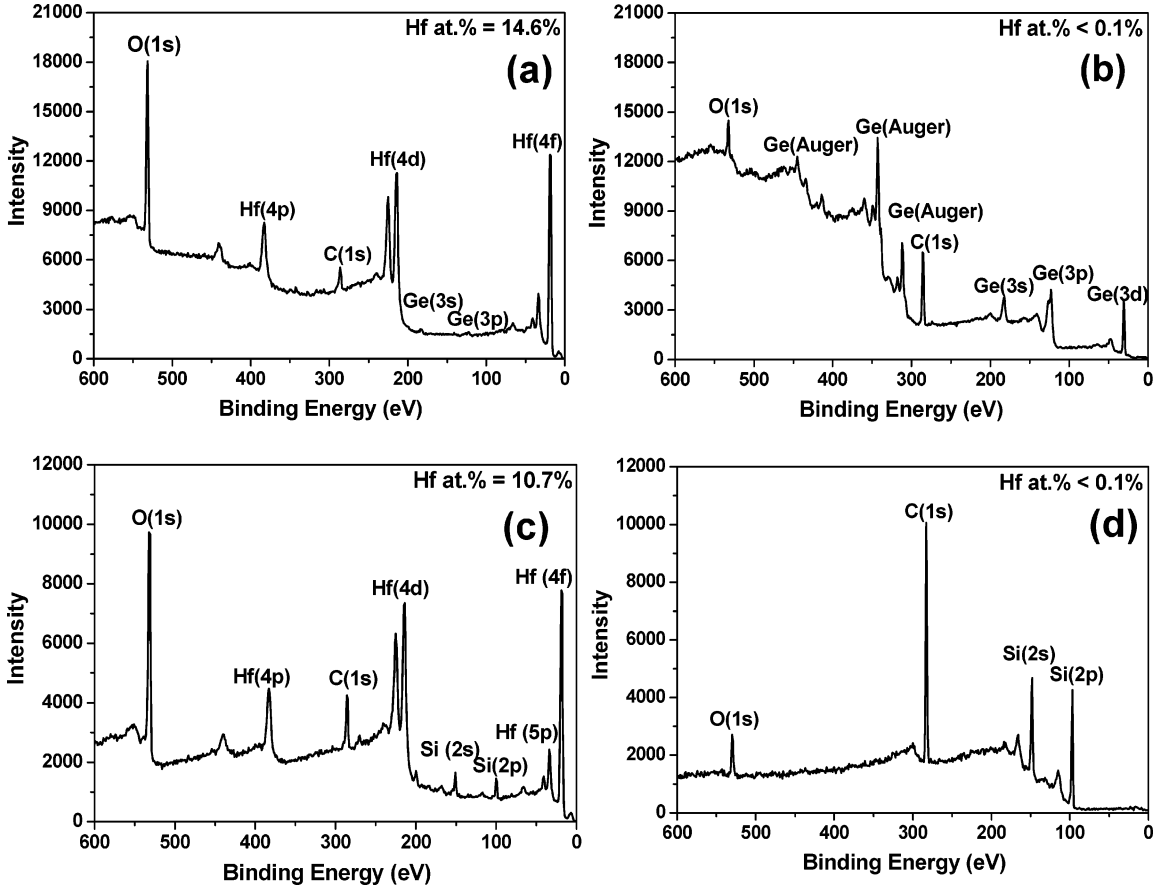

Figure 1. XPS survey spectra on (a) the reference Ge(100)-H substrate after HfO_2 ALD; (b) the octadecyl monolayer coated Ge(100) substrate after HfO_2 ALD; (c) the reference Si(100)-H substrate after HfO_2 ALD; and (d) the octadecyl-coated Si(100) substrate after HfO_2 ALD. Hf atom % composition values are shown in the upper right corners.

hydride-terminated substrates by 1-octadecene using the thermal method described above, with an exposure time of 120 min. The octadecyl-coated surfaces, together with hydrogen-terminated reference samples, were introduced into the ALD reactor and subjected to 50 HfO_2 ALD cycles. XPS studies carried out on the substrates following HfO_2 ALD are shown in Figure 1. Figure 1 compares the XPS spectra for the unmodified hydrogen-terminated Ge(100) and Si(100) surfaces with those for octadecyl-terminated Ge(100) and Si(100). Within the sensitivity of the spectrometer (0.1 atom %), it is evident that there are no Hf peaks on the octadecyl-coated Ge surface [Figure 1b] while significant HfO_2 was deposited on the Ge(100)-H reference substrate [Figure 1a]. Similar results were observed on the Si(100) surface. No hafnium peaks were measured on the 1-octadecene deactivated Si [Figure 1c] substrate while significant HfO_2 is observed on the Si(100)-H reference sample [Figure 1d] in the same ALD run. Moreover, the same results are found by XPS on 1-octadecene deactivated Ge(111)-H and Si(111)-H substrates (data not shown): no HfO_2 is deposited on the monolayer-passivated Ge(111) and Si(111) surfaces while HfO_2 is deposited in the nonpassivated, hydrogen-terminated samples. These results demonstrate that 1-octadecene can be applied as an effective molecular resist precursor against ALD of HfO_2 high-κ dielectric films.

The ability of octadecyl-covered Ge and Si to resist Pt ALD was also investigated. The requirements on a Pt ALD resist are expected to be less stringent than those for HfO_2, for the following reason. From previous studies, we have found that metal oxide ALD processes such as that for HfO_2 are relatively easy to nucleate and, in turn, difficult to deactivate, requiring very high quality monolayer resists.[18−20] On the other hand, it is found that metal ALD processes are relatively difficult to nucleate and hence easier to block.[33] In other words, if an organic monolayer resist can successfully block metal oxide ALD, it is likely to completely block ALD of a metal such as Pt. Consistent with this expectation, we observed that the Pt ALD process could be completely deactivated for at least 75 cycles by octadecyl monolayers formed on hydrogen-terminated Ge [Ge(100)-H and Ge(111)-H] and hydrogen-terminated Si [Si(100)-H and Si(111)-H] samples under the same conditions described above (results not shown).

All the results discussed above were obtained under thermal reaction conditions. UV reaction has also been explored as the other method for monolayer formation, and similar results were obtained. Both octadecyl- and dodecenyl-functionalized Si and Ge substrates were formed by UV reaction with 1-octadecene and 1-dodecyne, respectively, for 2 h. Under these UV radiation conditions, monolayers formed by both 1-octadecene and 1-dodecyne led to complete deactivation against HfO_2 and Pt ALD. We did not carry out as comprehensive an analysis on the dependence of time for

(33) Park, K. J.; Doub, J. M.; Gougousi, T.; Parsons, G. N. *Appl. Phys. Lett.* **2005**, *86*, 51903.

Table 1. WCA and Film Thickness for Reaction of 1-Octadecene on the Ge(100)-H Sample before ALD,and XPS Elemental Analysis after HfO_2 ALD

reaction time (min)	static WCA (deg)	thickness of organic film (Å)	element atom % XPS analysis after HfO_2 ALD	
			Hf	C
0	N/A[a]	1.7 ± 0.4[b]	12.6	19.1
30	103.8 ± 1.9	18.7 ± 2.1	9.7	21.7
60	105.3 ± 1.2	20.9 ± 1.7	6.8	28.6
90	107.2 ± 1.0	23.1 ± 1.1	2.5	41.9
120	109.2 ± 0.7	24.8 ± 0.6	<0.1	50.7

[a] Because the hydrogen-terminated sample is very easily oxidized, the contact angle is not accurate for the Ge−H surface. [b] This measurement likely reflects possible surface carbon contamination or a partially oxidized sample formed under ambient conditions prior to XPS analysis.

the UV reaction as for the thermal reaction. However, samples generated with shorter reaction time (e.g., 1 h of UV reaction) demonstrated submonolayer film formation behavior and were not able to fully deactivate the ALD processes. Similarly, monolayers formed by UV reaction using shorter chain length molecules (e.g., 1-octene) were also unable to fully block ALD. Each of these results is consistent with the corresponding study using thermal monolayers.

2. Effect of Monolayer Formation Time on Chemical Properties. To help understand the blocking mechanism of the monolayers formed by hydrosilylation and hydrogermylation, a time dependence study of octadecyl monolayer formation was carried out. The results on Ge(100)-H samples under thermal reaction with 1-octadecene solutions are summarized in Table 1. For different reaction times, the film properties (WCA, thickness) and the results of a post-ALD elemental analysis are compared in Table 1. The hydrophobicity, the thickness of the organic films, and the C atom % increase with increasing reaction time. These properties, however, have been found to be less sensitive to the quality of the monolayer than is the ALD blocking efficiency.[18] The Hf atom % measured after the ALD process is a good measurement for assessing the blocking effectiveness of a particular film. It is apparent from Table 1 that it took approximately 2 h for the full monolayer resists to form and to achieve complete deactivation. A similar time-dependent study was also carried out using Pt ALD. However, even for the shortest monolayer formation time, no Pt was detectable within the XPS detection limit (atom % < 0.1%) compared to detectable Pt (Pt atom % = 1.8%) observed on the reference Si-H (0 min) sample after the same ALD run. This result indicates that even poor monolayers are effective at blocking Pt ALD.

The WCA, film thickness, and Hf atom % for the HfO_2 ALD experiments are plotted in Figure 2 as a function of reaction time. Interestingly, the functional form of this graph differs from that of the ALD resists based on siloxane SAMs studied previously.[18] For the alkene-based monolayers studied here, the WCA and film thickness are both proportional to the reaction time, as shown in Figure 2, while the Hf atom % drops linearly with time. In the previous case, however, the WCA and film thickness values rise quickly and then plateau with time, while complete deactivation is only achieved at the latest stages of SAM formation.[18] This nonlinear behavior in the siloxane SAMs was attributed to

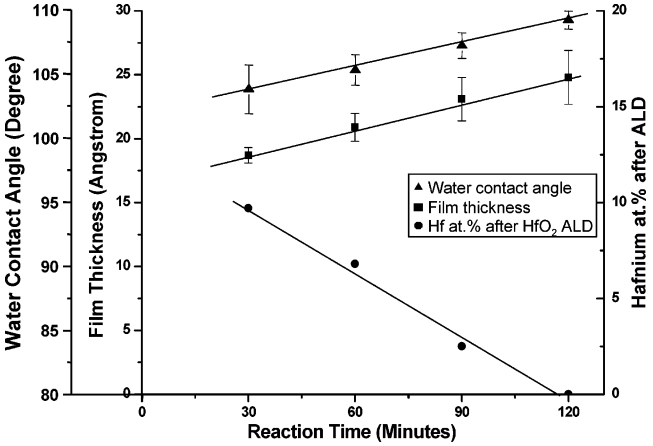

Figure 2. Time dependence of octadecyl film formation and its ALD blocking effect for HfO_2 ALD on the Ge(100) surface. WCA, film thickness, and Hf atom % are plotted versus thermal reaction time.

rapid formation of a porous monolayer, followed by a long period (about 2 days) necessary to completely fill in pinholes in the SAM film.

Both high resolution XPS and AFM measurements were carried out on partly formed monolayer samples before and after ALD to gain further insight into the blocking mechanism. According to Table 1, 90 min of thermal reaction of 1-octadecene results in a submonolayer coverage film that is not completely protective of the surface against ALD. An XPS survey scan on a Ge sample that was subjected to HfO_2 ALD after 90 min thermal reaction with 1-octadecene is shown in Figure 3a. By comparison with Figure 1a [H-terminated Ge(100)], it is evident that while deposition does occur, there is less HfO_2 (Hf atom % = 2.5%) observed on the partly blocked sample than on the unblocked reference sample (Hf atom % = 12.6%).

More detailed information can be obtained by examining the Si and Ge XPS peaks at higher resolution, because photoelectrons from the core levels are very sensitive to the surrounding chemical environment. Fine scans of the Ge 3d peaks were taken on the full monolayer (120 min) and submonolayer (90 min) samples and are shown in Figure 3b in solid and dashed curves, respectively. Samples with shorter alkene reaction times were not analyzed because the correspondingly thicker HfO_2 films deposited on these samples led to larger Hf 4f plasmon peaks which interfered with the Ge 3d peaks. For the spectrum of the full monolayer-covered sample, a single peak is observed at ~30 eV, corresponding to germanium covalently bonded to carbon, and no obvious GeO_x component appears in the higher binding energy region (~33 eV) even after annealing to high temperature (300 °C). In contrast, in the spectrum of the submonolayer-covered sample, a high binding energy peak clearly appears as a shoulder on the carbon-bonded Ge peak; this higher energy peak indicates the presence of GeO_x.[34] It is likely that this new peak is a result of oxidation of the Ge substrate where it is not fully passivated with the alkene.

A similar analysis was performed on the Si 2p peaks, which are compared in Figure 3c. The lower dashed spectrum

(34) Moulder, J.; Stickle, W. F.; Sobol, P. E.; Bomben, K. D. *Handbook of X-ray Photoelectron Spectroscopy*, 2nd ed.; Perkin-Elmer Corp. (Physical Electronics Division): Wellesley, MA, 1992.

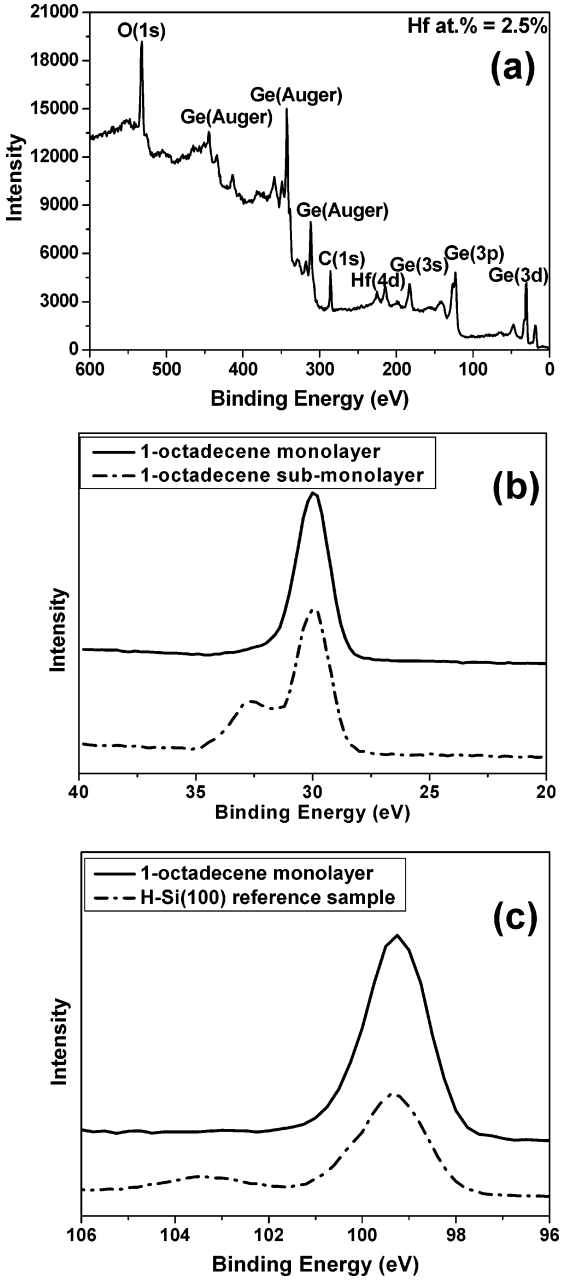

Figure 3. XPS spectra after HfO_2 ALD. (a) Survey scan of octadecyl submonolayer (after 90 min thermal reaction) formed on Ge(100)-H. (b) Ge 3d peak fine scan of monolayer (solid curve) and submonolayer (dashed curve) resists formed on Ge(100)-H. (c) Si 2p peak fine scan of reference Si(100)-H sample (solid curve) and octadecyl-monolayer passivated Si(100) samples (dashed curve).

of Figure 3c is the Si 2p fine scan of the reference hydrogen-terminated silicon substrate after HfO_2 ALD. Two distinct peaks are clearly evident in the spectrum: a higher binding energy peak near 103 eV is shifted 3−3.5 eV up from a lower binding energy peak, which is attributed to a bulk Si 2p peak. Analogous to the germanium XPS peaks, the higher binding energy peak is assigned to oxidized silicon. For the octadecyl monolayer passivated sample (Figure 3c top solid spectrum), only the single, lower binding energy Si 2p XPS peak is present, confirming the absence of SiO_2 formation after the ALD process. We note that the Si−C binding energy is around 100 eV, which is near the bulk Si 2p peak (∼99 eV).[34] With the equipment resolution, it is difficult to deconvolute the Si−C peak from the bulk Si 2p peak. Therefore, only one single low energy peak is resolved for the octadecyl-passivated sample.

Both the Si and Ge XPS fine scans studies confirmed that these non-oxide semiconductors can be fully passivated by octadecyl monolayers and that these monolayer resists are very stable during the ALD process.

The AFM images shown in Figure 4 compare the surface morphology observed for full and partial octadecyl monolayers before and after ALD. Figure 4a is taken on a full monolayer formed after 2 h of thermal reaction of 1-octadecene on a Ge(100)-H substrate, while Figure 4b shows a submonolayer formed after 1 h of thermal reaction. The full monolayer film (Figure 4a) demonstrates a very smooth surface with a root-mean-square roughness of ∼1 Å, whereas it is clear from Figure 4b that the submonolayer sample contains many regions with large height variations. A sectional analysis of the submonolayer sample indicates that the vertical difference (*z* direction) between the dark and the light regions is about 2.5 nm, which is consistent with the length of an 18-carbon hydrocarbon chain. This result suggests that the surface contains a significant amount of exposed, nonreacted areas, surrounded by octadecyl-terminated regions of the surface. These nonreacted areas are likely sites for precursor nucleation and subsequent film growth.

To examine the effect of these open regions, AFM analysis was performed immediately after the HfO_2 ALD process. For the full-monolayer sample, the surface showed no noticeable change and was still very smooth with ∼1 Å surface roughness. For the submonolayer sample, we observed a similar structure [Figure 4c] as for the sample before ALD, with regions exhibiting different heights over areas extending ∼100 nm. However, the vertical difference after ALD is only about 1 nm, compared to 2.5 nm before ALD. We propose that the smaller height variation reflects film growth by ALD in the open regions. As mentioned previously, the 50 cycles of HfO_2 ALD will deposit 3.6−3.8 nm HfO_2. If the exposed regions are the nucleation sites, ∼3.6 nm of HfO_2 will deposit there, leading to ∼1 nm vertical difference between the film and the surrounding 2.5 nm high octadecyl layer. We note that although the data shown in Figure 4 are for 1-octadecene reaction on Ge(100)-H, parallel experiments were performed on Ge(111)-H, and similar results were obtained. Although atomically resolved scanning tunneling microscopy studies showed differences in alkene reaction with hydrogen-terminated Si(111) and Si(100),[35−37] we have not observed any difference, which may due to the lower AFM resolution.

3. Other Alkenes and Alkynes. In addition to 1-octadecene, several other 1-alkenes and 1-alkynes with different tail lengths have also been investigated as resists against ALD. 1-Alkenes with chain lengths ranging from 8 to 18 carbon atoms were studied (1-octene, 1-decene, 1-dodecene, 1-tetradecene, 1-hexadecene, and 1-octadecene), while 8-

(35) Cicero, R. L.; Chidsey, C. E. D.; Lopinski, G. P.; Wayner, D. D. M.; Wolkow, R. A. *Langmuir* **2002**, *18*, 305.
(36) Lopinski, G. P.; Wayner, D. D. M.; Wolkow, R. A. *Nature* **2000**, *406*, 48.
(37) Pitters, J. L.; Wolkow, R. A. *J. Am. Chem. Soc.* **2005**, *48*, 127.

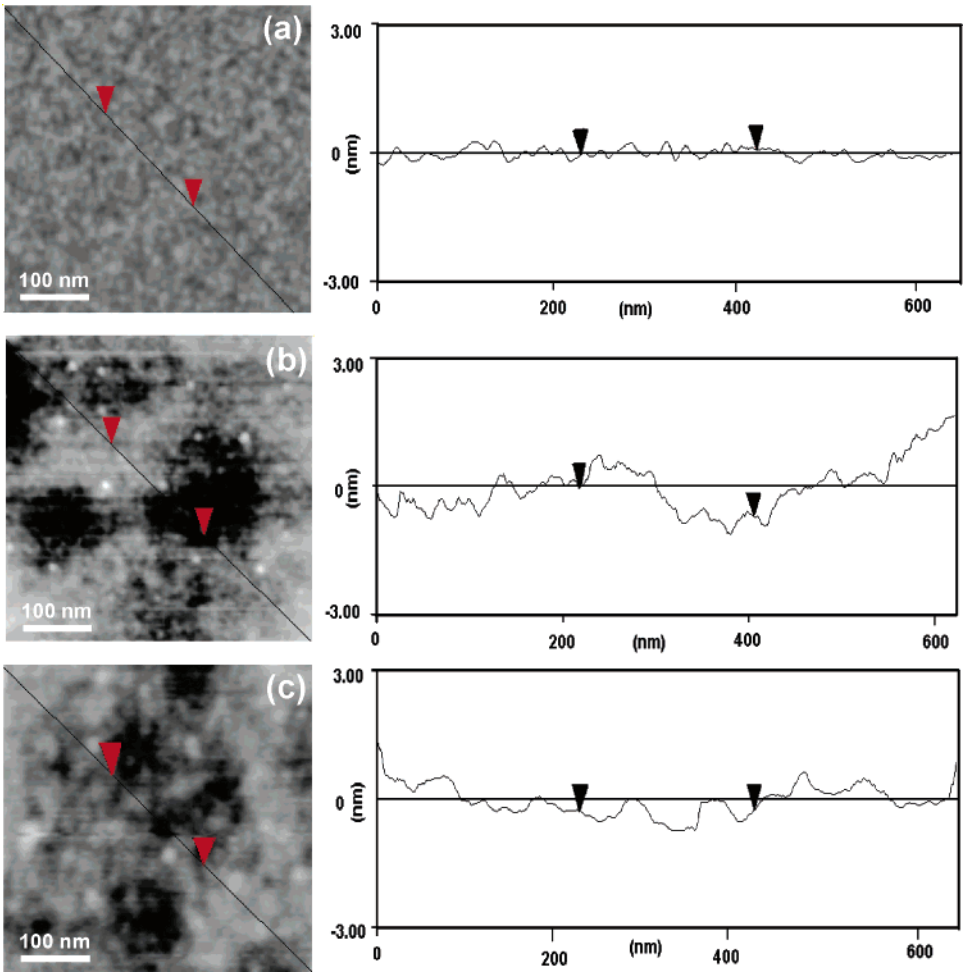

Figure 4. AFM study on (a) the octadecyl monolayer on Ge(100); (b) the octadecyl submonolayer on Ge(100); and (c) the octadecyl submonolayer on Ge(100) after HfO_2 ALD. In each case, the monolayers were formed by thermal reaction of 1-octadecene with Ge(100)-H

Table 2. WCA and Film Thickness for Reaction of Different 1-Alkenes and 1-Alkynes on the Ge(100)-H Sample before ALD and XPS Elemental Analysis after HfO_2 and Pt ALD

sample description (organic monolayer on Ge(100)−H)		static WCA (deg)	thickness of organic film (Å)	element atom % XPS analysis after HfO_2 ALD		element atom % XPS analysis after Pt ALD	
				Hf	C	Pt	C
1-alkenes (C_nH_{2n})	1-octadecene	109.2 ± 0.7	24.8 ± 0.6	<0.1	50.7	<0.1	50.4
	1-hexadecene	108.9 ± 1.1	22.5 ± 1.3	<0.1	47.7	<0.1	47.2
	1-tetradecene	108.4 ± 0.9	20.1 ± 1.1	<0.1	44.2	<0.1	44.9
	1-dodecene	107.3 ± 0.7	18.3 ± 0.8	0.2	41.7	<0.1	42.2
	1-decene	105.1 ± 1.3	15.5 ± 0.7	1.2	38.6	<0.1	39.1
	1-octene	103.6 ± 1.2	13.8 ± 1.1	2.6	35.5	<0.1	37.4
1-alkynes (C_nH_{2n-2})	1-dodecyne	108.7 ± 0.6	18.2 ± 0.7	<0.1	42.8	<0.1	42.8
	1-decyne	105.8 ± 1.5	15.7 ± 1.3	1.0	39.4	<0.1	40.6
	1-octyne	104.0 ± 2.1	13.6 ± 0.9	2.5	36.3	<0.1	38.3
none		N/A[a]	1.7 ± 0.4[b]	12.6	19.1	1.8	17.6

[a] Because the hydrogen-terminated sample is very easily oxidized, the contact angle is not accurate for the Ge−H surface. [b] This measurement likely reflects possible surface carbon contamination or a partially oxidized sample forzmed under ambient conditions prior to XPS analysis.

to 12-carbon-chain 1-alkynes were included (1-octyne, 1-decyne, and 1-dodecyne). The results are summarized in Table 2, indicating the WCA and film thickness as well as the elemental analysis after HfO_2 ALD and Pt ALD for each molecule.

For both the alkenes and the alkynes, the hydrophobicity, the thickness of the organic films, and the C atom % are all found to increase with increase in the alkyl chain length, while the Hf atom % measured after the HfO_2 ALD process decreases. When the length of the alkyl chain exceeds 12 carbons, the Hf atom % after ALD drops to below the detection limit. The data show that when the alkyl chain is sufficiently long, the monolayer resists can completely block the HfO_2 ALD process. These results are consistent with our previous study of *n*-alkyltrichlorosilane based ALD resists.[20] In that case, the dodecyl (12 carbon atoms) group was also the minimum tail length for which HfO_2 ALD could be fully deactivated.[20] The data in Table 2 indicate that both 1-alkenes and 1-alkynes can form monolayer resists on the Ge(100)-H substrates. For the same chain length, 1-alkenes and 1-alkynes form monolayers with similar film properties and similar deactivating efficiencies.

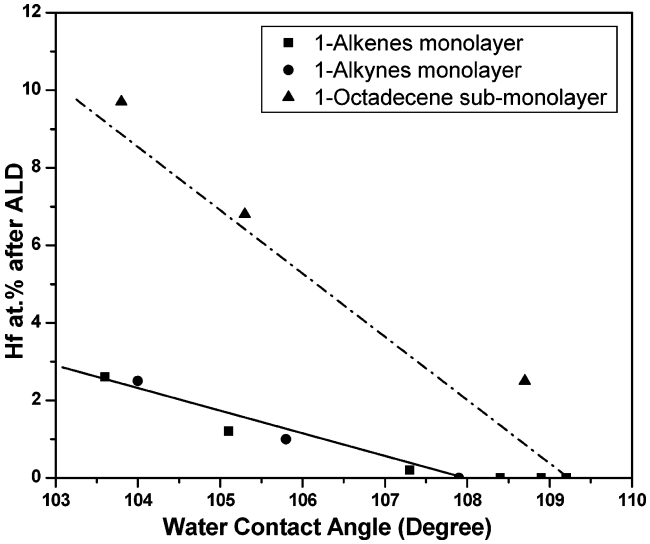

Figure 5. Plot of the Hf atom % post-ALD versus WCAs measured for a variety of samples before the ALD process. The Hf atom % is a measure of the blocking efficiency toward the ALD process.

Although there is a minimum chain length for which the 1-alkenes and 1-alkynes can provide complete blocking of the HfO_2 ALD process, all chain lengths studied produced effective resists against Pt ALD. The difference reflects the higher difficulty in nucleating Pt compared to HfO_2. Because Pt ALD requires a more active starting surface for nucleation, samples coated with monolayers containing tail groups as short as eight carbon atoms long are still sufficiently hydrophobic to completely prevent nucleation. Thus they are all efficient resists for Pt ALD.

A plot of the hafnium atomic percentage after the HfO_2 ALD process versus WCA before the ALD process has been constructed for all of the deactivating agents examined in this study. The resulting plot is shown in Figure 5. Some interesting correlations between Hf atom % and WCA are apparent in the figure. The Hf atom % measured after the ALD process is a good measurement of the deactivation effectiveness of the film. There is a general trend showing better deactivation efficiency with increasing hydrophobicity (WCA) for all the samples investigated in this study. For both 1-alkene (squares) and 1-alkyne (dots) full monolayers, the Hf atom % is negatively dependent upon the WCA values, as fitted by a solid line in Figure 5. For the submonolayer resists (triangles), interestingly, the Hf atom % is also negatively dependent on the hydrophobicity, but with a steeper slope as fitted by the dashed line. This observation is quite different from the previous alkyltrichlorosilane-based monolayer resists.[20] In the previous case, there was a clear difference in deactivation potential (Hf atom %) for the densely packed SAMs compared to the poorly packed SAMs. Only densely packed SAMs showed a deactivation efficiency that was negatively dependent on the WCA, whereas the loosely packed SAMs did not follow any clear trends.[20] These differences are discussed below.

4. Discussion of Mechanism. We now discuss the experimental results in the context of a proposed deactivation mechanism for the alkyl- and alkenyl-based monolayer. It is evident from the data in Figure 1 that, under the right formation conditions, the octadecyl monolayer acts as an effective resist against ALD of both dielectric and metal films. As illustrated in Scheme 1, the general process is one in which the monolayer prevents film deposition by inhibiting nucleation and subsequent growth steps. To investigate this mechanism in more detail, we focus on HfO_2 ALD because the data indicate that HfO_2 ALD is more sensitive to the quality of the monolayer resists and more difficult to deactivate than Pt.

Nucleation of HfO_2 using $HfCl_4$ and water precursors is believed to occur at surface hydroxyl groups; however, for ALD with $Hf(N(CH_3)_2)_4$ and water precursors, the nucleation of HfO_2 may occur directly on hydrogen-terminated substrates in addition to hydroxyl sites.[4,38] Hence, one important role of the monolayer resists on these non-oxidized semiconductor substrates is likely that they remove surface active sites and prevent the oxidization of the substrate, thus hindering HfO_2 ALD nucleation at the interface. In addition, the hydrocarbon tails likely block penetration of the precursor to the surface, where they might otherwise react with any defect nucleation sites. A similar mechanism was proposed for siloxane SAM resists on SiO_2 surfaces.[20]

Given the role of the monolayer in protecting the surface from oxidation and precursor exposure, we would expect that only well-packed monolayers with sufficiently long chains could provide complete ALD blocking. If the 1-octadecene does not form a densely packed monolayer, the substrate may become oxidized through openings in the monolayer during the ALD process, leading to nucleation and growth of HfO_2 at those nonpassivated regions. Such a result was observed previously on imperfect monolayers of octadecyltrichlorosilane resists on SiO_2 substrates, in which ALD did occur.[18] The results of Table 1 show that, indeed, longer hydrosilylation or hydrogermylation times are necessary to fully deactivate the HfO_2 ALD process.

On the other hand, the detailed time-dependent behavior observed here differs from that of alkyltrilchlorosilane-type SAMs on oxide substrates. For the alkene-based monolayers, the WCA and film thickness increase linearly and Hf atom % decreases linearly with reaction time (Figure 2), leading to a strong inverse correlation between WCA (film thickness) and Hf atom %. In contrast, for the octadecyltrichlorosilane resists, the WCA and film thickness values rise quickly and then plateau with time, with complete deactivation achieved only at the latest stages of SAM formation.[18] WCA alone is not a good indicator of resistance against ALD in this case. We suggest that the difference can be explained by the different film formation mechanisms between these two types of monolayers.

The trichlorosilane-based precursors typically polymerize in solution, forming small clusters before binding to hydroxyl groups on the oxide substrate.[39,40] Pinholes are expected to form between the spaces of those adsorbed clusters. The nonlinear behavior in the siloxane SAMs was, therefore, attributed to rapid formation of a porous monolayer, followed

(38) Ho, M. T.; Wang, Y.; Brewer, R. T.; Wielunski, L. S.; Chabal, Y. J.; Moumen, N.; Boleslawski, M. *Appl. Phys. Lett.* **2005**, *87*, 133103.
(39) Bunker, B. C.; Carpick, R. W.; Assink, R. A.; Thomas, M. L.; Hankins, M. G.; Voigt, J. A.; Sipola, D.; de Boer, M. P.; Gulley, G. L. *Langmuir* **2000**, *16*, 7742.
(40) Wang, Y.; Lieberman, M. *Langmuir* **2003**, *19*, 1159.

by a long period (about 2 days) necessary to completely fill in pinholes in the SAM film. We postulate that the rate-limiting step at long times is transport of the SAM precursor through the film. For the siloxane SAM case, the number and the size of the pinholes in the resist film determine the amount of HfO_2 deposited on the substrate during ALD.[18] However, it is likely that most of the pinholes are too small to affect the macroscopic WCA measurement, and hence there is no general correlation between the WCA values and the Hf atom % after ALD.

In contrast, the mechanism of film formation is very different for alkenes reacting with hydrogen-terminated Si or Ge. Hydrosilylation and hydrogermylation are radical reactions.[25,27,28,41,42] For hydrosilylation, a mechanism has been suggested for the film growth in which a silyl radical attacks the 1-alkene to form the Si−C bond, and a radical center on the α-carbon atom is formed. This kinetic chain propagates by abstraction of a H atom from the nearest-neighbor Si atom by the β carbon-centered radical. According to such a mechanism, the monolayer grows by addition of 1-alkenes to the end of a kinetic chain, which propagates across the surface, rather than stepwise at random individual Si sites.[27,36] A similar reaction mechanism is also found for hydrogermylation.[25,28]

Therefore, for 1-octadecene, the rate-limiting step under typical film formation conditions is radical generation at the substrate; the film initiates from the radical generation sites and spreads outward through propagation, while unreacted regions start to shrink. At early stages of monolayer formation, this type of film growth mechanism will result in a combination of some regions completely covered with the monolayer, with other regions that are free of the organic monolayer. The resulting film structure is evident in the AFM image of Figure 4, which shows unpassivated regions a few hundred nanometers to a micrometer in size. These large unreacted, hydrophilic regions will affect the WCA values as well as the ALD process, leading to a correlation between the hydrophobicity and ALD deactivating efficiency.

The data in Figure 5 are also consistent with the deactivation mechanism that was proposed in Scheme 1. For the densely packed, long-chain alkyl monolayers (solid markers), the surface is completely passivated and the monolayer resists prevent the substrate from oxidizing during the subsequent ALD process. The hydrophobic surface increases the incubation time of both HfO_2 and Pt ALD processes and also prevents the penetration of ALD precursors into the film, where it might reach defects at the interface that act as nucleation sites. Even for densely packed monolayers, however, a minimum chain length is required. A short alkyl tail group does not provide sufficient hydrophobicity, and the interface may become oxidized or Hf metal precursors or water may still be able to penetrate into the surface and grow via defects at the interface.

For the submonolayer films (triangles in Figure 5), the AFM data show that there are regions of the surface up to 1 μm in size that are unpassivated. These regions can oxidize and provide nucleation sites for the ALD process. Unlike depositions on densely packed monolayers, these large regions are more conducive to the nucleation of ALD precursors. Consequently, films are easier to nucleate and faster to grow. This explains the significantly larger Hf atom % at all WCAs for the submonolayer samples compared to the full-monolayer case, corresponding to poorer deactivation effectiveness overall.

Conclusions

In summary, we have carried out a study evaluating the use of 1-alkenes and 1-alkynes for a new type of monolayer resist on hydrogen-terminated germanium and silicon semiconductor surfaces. A series of 1-alkenes and 1-alkynes with different chain lengths were explored as deactivating agents for ALD of HfO_2 and Pt films. It is shown that to achieve satisfactory deactivation toward HfO_2 ALD, it is necessary to form densely packed, highly hydrophobic monolayer resists at least 12 carbon atoms long, whereas for Pt ALD, the shortest tail group studied, 8 carbons, is sufficient to achieve full deactivation. A mechanism for the film formation and blocking process is discussed and compared with alkylsilane-based SAM resists.

With the successful development of monolayer ALD resists on non-oxide semiconductor substrates comes the possibility of using them for area-selective ALD. Area-selective ALD can be achieved either by selective adsorption[29] of the monolayer on one region of a patterned substrate over another or by patterning the resists[25,41,43−47] after they are formed. The final removal of the monolayer resists after completion of the selective ALD process might be achieved by thermal decomposition under hydrogen gas flow or ozone plasma.

Acknowledgment. We thank Hyoungsub Kim, Raghavasimhan Sreenivasan, and Paul C. McIntyre for insightful discussion and David W. Porter, Sandeep Giri, and Xirong Jiang for their help on Pt ALD. This work was supported in part by the NSF/SRC Center for Environmentally Benign Semiconductor Manufacturing (No. EEC9528813), the Stanford Initiative for Nanoscale Materials and Processes, and the Center for Integrated Systems. R.C. acknowledges Texas Instruments for a graduate fellowship.

CM0607785

(41) Sieval, A. B.; Linke, R.; Zuilhof, H.; Sudholter, E. J. R. *Adv. Mater.* **2000**, *12*, 1457.
(42) Sieval, A. B.; van den Hout, B.; Zuilhof, H.; Sudholter, E. J. R. *Langmuir* **2000**, *16*, 2987.
(43) Buriak, J. M. *Adv. Mater.* **1999**, *11*, 265.
(44) Lee, E. J.; Ha, J. S.; Sailor, M. J. *J. Am. Chem. Soc.* **1995**, *117*, 8295.
(45) Shirahata, N.; Masuda, Y.; Yonezawa, T.; Koumoto, K. *J. Eur. Ceram. Soc.* **2004**, *24*, 427.
(46) Stewart, M. P.; Buriak, J. M. *Angew. Chem., Int. Ed.* **1998**, *37*, 3257.
(47) Sun, S. Q.; Chong, K. S. L.; Leggett, G. J. *Nanotechnology* **2005**, *16*, 1798.